





RESEARCH ARTICLE | APRIL 03 2023

On the incorporation of conservation laws in machine learning tabulation of kinetics for reacting flow simulation

Thomas Readshaw ; W. P. Jones ; Stelios Rigopoulos  



Physics of Fluids 35, 047103 (2023)

<https://doi.org/10.1063/5.0143894>



View
Online



Export
Citation

CrossMark

On the incorporation of conservation laws in machine learning tabulation of kinetics for reacting flow simulation

Cite as: Phys. Fluids **35**, 047103 (2023); doi: 10.1063/5.0143894

Submitted: 27 January 2023 · Accepted: 12 March 2023 ·

Published Online: 3 April 2023



View Online



Export Citation



CrossMark

Thomas Readshaw, W. P. Jones, and Stelios Rigopoulos^{a)}

AFFILIATIONS

Department of Mechanical Engineering, Imperial College London, Exhibition Road, London SW7 2AZ, United Kingdom

^{a)} Author to whom correspondence should be addressed: s.rigopoulos@imperial.ac.uk

ABSTRACT

Tabulation of chemical mechanisms with artificial neural networks (ANNs) offers significant speed benefits when computing the real-time integration of reaction source terms in turbulent reacting flow simulations. In such approaches, the ANNs should be physically consistent with the reaction mechanism by conserving mass and chemical elements, as well as obey the bounds of species mass fractions. In the present paper, a method is developed for satisfying these constraints to machine precision. The method can be readily applied to any reacting system and appended to the existing ANN architectures. To satisfy the conservation laws, certain species in a reaction mechanism are selected as residual species and recalculated after ANN predictions of all of the species have been made. Predicted species mass fractions are set to be bounded. While the residual species mass fractions are not guaranteed to be non-negative, it is shown that negative predictions can be avoided in almost all cases and easily rectified if necessary. The ANN method with conservation is applied to one-dimensional laminar premixed flame simulations, and comparisons are made with simulations performed with direct integration (DI) of chemical kinetics. The ANNs with conservation are shown to satisfy the conservation laws for every reacting point to machine precision and, furthermore, to provide results in better agreement with DI than ANNs without conservation. It is, thus, shown that the proposed method reduces accumulation of errors and positively impacts the overall accuracy of the ANN prediction at negligible additional computational cost.

© 2023 Author(s). All article content, except where otherwise noted, is licensed under a Creative Commons Attribution (CC BY) license (<http://creativecommons.org/licenses/by/4.0/>). <https://doi.org/10.1063/5.0143894>

I. INTRODUCTION

Reacting flow simulation methods that involve the direct coupling of chemistry and flow require the real-time numerical integration of the chemical kinetics. The chemical kinetics are described by a system of ordinary differential equations (ODEs), where each ODE expresses the instantaneous net formation rate of one of the chemical species present in the mechanism. For detailed chemical mechanisms, this system of ODEs can quickly become large and unwieldy, and furthermore, such systems are often stiff, which is often the case for combustion mechanisms. It is the integration of these ODEs at every point in time and space during a simulation that is the computational bottleneck for reacting flow simulations if conventional integration techniques are used. Methods in which this computational bottleneck is present include, but are not limited to, transported probability density function methods,^{1–3} direct numerical simulation,^{4–6} Reynolds averaged Navier–Stokes (RANS) and unsteady RANS simulations,^{7,8} the thickened flame model,^{9,10} and partially

stirred reactors.^{11,12} In all of these methods, the computational cost of integrating the chemical kinetics precludes the use of extensive detailed mechanisms.

Chemical mechanism tabulation eases this computational bottleneck by storing the behavior of the reaction mechanism for a given region of composition space and performing retrievals during the simulation. However, the simplest tabulation techniques, such as the lookup table,¹³ grow exponentially in memory requirements with the dimension of the table and so cannot be feasibly stored on distributed memory computer architectures if more than a handful of reaction variables are considered. On-the-fly tabulation methods, such as the binary tree-based *in situ* adaptive tabulation¹⁴ (ISAT), alleviate this issue to some extent by only storing the composition space accessed in the application, although memory requirements can still increase as simulations progress if unfamiliar regions of the composition space are encountered. Flame regime-specific tabulation approaches, such as those which use the steady flamelet model¹⁵ or progress variable

approaches, generally have fast retrieval times and small memory requirements, but their application is limited to the intended regimes.

An alternative method to chemical mechanism tabulation uses artificial neural networks (ANNs), which are a class of machine learning tools capable of a wide variety of tasks. In the present work, the focus is on thermochemistry tabulation; hence, the ANNs employed are multi-layer perceptrons (MLPs), which are well suited to non-linear regression and so can approximate the function implicitly defined by the overall behavior of the system of ODEs. A data-driven non-linear optimization process, known as training, is used to teach the MLP to approximate the system of ODEs over a given region of composition space. Only the weights need to be stored during a simulation, so memory requirements are low. MLP retrievals are performed using a small number of matrix multiplications, thus reducing the required computational time. The proliferation of machine learning has led to a large number of recent applications in the context of combustion modeling, dealing with various aspects of the problem, a review of which can be found in Ihme *et al.*¹⁶ In the following, a brief review of works directly relevant to thermochemistry tabulation will be presented.

A class of works (such as Refs. 17–20) use ANNs to perform retrievals from mixture fraction/progress variable-based tables created using the steady flamelet model. As mentioned, such tabulation techniques already have fast retrieval times, with the main benefit of using the ANNs being the reduced memory required to store the weights compared to the original table. When it comes to ANNs employed in the context of combustion models that involve direct coupling of chemistry and flow, the first challenge is to ensure that training data are collected, which allows the ANNs to generalize to families of different combustion problems. This is a critical step in the ANN tabulation process, as the accuracy of MLPs extrapolating outside of the composition region on which they have been trained is poor. Approaches, which take training data from the application,²¹ would lead to good ANN accuracy but negate any potential speed-up from using the ANNs in the first place. The simplest approaches to generating training data carry out sampling from across the theoretically allowable composition space^{22–26} but are impracticable when considering larger mechanisms where the required composition space resolution would lead to a prohibitively large training set.

Using a canonical combustion problem to generate the training set provides data in relevant composition space regions which is not specific to a given application and can be used for mechanisms with a large number of species. Sen and Menon²⁷ and Sen *et al.*²⁸ used linear-eddy mixing simulations to generate training data before applying the resulting MLPs to large eddy simulations of syngas/air flames. Chatzopoulos and Rigopoulos,²⁹ Franke *et al.*,³⁰ Readshaw *et al.*,¹ and Ding *et al.*^{31,32} used unsteady laminar flamelets with ignition and extinguishing to generate training data, with subsequent successful application of the MLPs to a variety of non-premixed turbulent flames. Other canonical combustion problems used include stochastic micro-mixing systems^{33,34} for the simulation of syngas turbulent oxy-flames, perfectly stirred reactors,³⁵ and eddy dissipation simulations.³⁶ Alternatively, at a modest computational cost, the MLPs can be trained on-the-fly,³⁷ in an analogous manner to ISAT.

The second challenge when tabulating thermochemistry using ANNs is to ensure good prediction accuracy in a given application using the simplest ANN architecture possible. Although accuracy

generally increases with the number of ANN parameters available, retrieval times will also increase and so the potential speed-up will diminish. Using fewer ANN parameters also allows the use of potentially more accurate but also more computationally intensive quasi-second-order or second-order training algorithms, such as the Levenberg–Marquardt algorithm. ANN architectures that use a single MLP to predict each species^{1,38} or extensions, such as the multiple MLP (MMLP) method,^{31,32} occupy a sweet spot where potential accuracy is high, but the number of parameters is relatively low.

The third challenge, which we attempt to tackle in this work (and was also identified in the review of Ihme *et al.*¹⁶), is to ensure that ANNs are physically consistent with the reacting systems they are used to approximate. Specifically, in the case of chemical mechanism tabulation, the laws of mass and element conservation and the bounds on the species mass fractions should be satisfied. Although out-of-bounds mass fractions can be clipped and mass conservation errors can be rectified by normalizing the predicted composition, element conservation errors are more difficult to rectify. As a result, strategies, such as random data generation,^{1,31,32} have been developed in conjunction with the MMLP method to essentially incorporate data with element conservation errors into the MLP training dataset. While such random data generation strategies have been successfully applied along with the MMLP method to a variety of premixed and non-premixed flames, they require the selection of allowable windows for the element ratios in the randomization process, which may not be easy to obtain ahead of time.

The element conservation laws manifest themselves as a series of linear constraints on the ANN outputs. In the context of atmospheric modeling, Beucler *et al.*³⁹ recently proposed a method for guaranteeing that ANN predictions satisfy certain linear constraints by predicting all but one variable and then appending a fixed “constraint layer” to their ANN. The constraint layer calculates the final value of a certain variable such that a linear constraint is satisfied. This method allows the constraint to be applied during the ANN training, thus leading to both physical consistency and good accuracy. However, fixing the constraint during training means that the variable that is associated with the constraint layer is also fixed. This presents a difficulty for chemical kinetics, where the choice of variable may depend on the local composition. This is because the inevitable errors in the ANN predictions may lead to different species at different locations being no longer bounded.

Therefore, it is advantageous to construct a method that applies the constraints as a post-processing step, for example, as performed by Bolton and Zanna,⁴⁰ again in the context of atmospheric modeling. Applying the constraints as a post-processing step allows flexibility regarding which variables to correct via the constraint, but also introduces the problem of choosing these variables. Wan *et al.*^{33,41} used a post-processing step to apply constraints in the context of reaction mechanisms, using an element conservation scheme to ensure that the predictions of 11 species in a reduced mechanism satisfy the element conservation laws in the full mechanism from which the reduced one was derived. While this approach was successful in satisfying the conservation laws, the limited number of species used meant that a manual selection of species for applying the element conservation correction was feasible.

In the present paper, we propose a method for automatically and robustly selecting which species to recalculate in order to ensure that

conservation laws are satisfied, for an arbitrary chemical mechanism. Once these species are selected, their values can be corrected in order to satisfy the mass and element conservation laws to machine precision. The method is formulated in such a way that the likelihood of unbounded predictions is very small. We also propose a method for rectifying unbounded predictions in the unlikely event of an unbounded corrected species. The proposed methodology can be easily appended to the existing ANN architectures for tabulation of chemical kinetics to incorporate the conservation laws in applications. The implementation presented here augments the MMLP methodology, which has been shown to yield very good predictions in laminar flamelets, one-dimensional laminar premixed flames, and turbulent flames with both fuels and fuel blends,^{1,31,32} all without employing data from the target problem in the training set. For this reason, no turbulent flame simulations will be carried out here; the objective is to show how the proposed approach can improve the conservation properties of the kinetics tabulation such that the simulations can acquire either more accuracy where this is needed or can be performed more efficiently by achieving similar accuracy with a simpler ANN.

Section II explains how a chemical mechanism is tabulated with ANNs, as well as the constraints that should be applied to the ANN predictions. In Sec. III, the proposed conservation method is outlined, with algorithms given to allow the computational implementation of the method. In Sec. IV, the conservation method is applied to the GRI 1.2⁴² and USC Mech II⁴³ combustion mechanisms, respectively, in the context of simulations of one-dimensional CH₄/air and C₃H₈/air laminar premixed flames with non-equal diffusivities. The effect of satisfying the constraints on ANN accuracy and speed-up is examined by comparing simulations with and without conservation to the direct integration simulations.

II. FUNDAMENTALS OF ANN TABULATION OF THERMOCHEMISTRY

The state of a mixture of ideal gases can be fully described by the concentrations of the constituent species and two thermodynamic state variables. If the pressure is fixed, then the state of the mixture is defined by $[h, Y_i]$, where h is the specific enthalpy (including both sensible and formation enthalpies), and Y_i are the mass fractions of the N_{sp} being considered. For a given initial state, the numerical integration of the system of chemical kinetics ODEs over a time step, Δt , yields the following mapping from the initial to final state:

$$[h(t), Y_i(t)] \mapsto Y_i(t + \Delta t), \tag{1}$$

where h does not change across the reaction step. This relationship can also be written in terms of the change in the species mass fractions over the time step being considered,

$$[h(t), Y_i(t)] \mapsto \Delta Y_i, \tag{2}$$

where $\Delta Y_i = Y_i(t + \Delta t) - Y_i(t)$. In either case, the mapping is determined by the chosen reaction mechanism. When using MLPs for thermochemistry tabulation, the initial state is treated as an input to the MLP and the final state (or the change) as an output, and the aim is to approximate the mapping from input to output as accurately as possible.

The first step in the MLP tabulation process is to generate a dataset suitable for the desired application, consisting of many input/output pairs in the form of Eq. (1) or Eq. (2). To enable more effective

MLP training, several manipulations of the input variables may be employed. These include simple linear scaling, non-linear operations, such as log or root transforms, or dimension reduction techniques, such as principal component analysis. If the transformed inputs are denoted by $r_j(t)$, where $j = 1, 2, \dots, N_{inputs}$, and the transformed outputs are denoted as s_k , where $k = 1, 2, \dots, N_{outputs}$, then the mapping described by Eq. (1) or Eq. (2) becomes

$$r_j \mapsto s_k. \tag{3}$$

Figure 1 shows a generic MLP with K outputs, consisting of neurons (circles) arranged in layers that are joined together with connections (lines), each of which has an associated weight. The number of layers, the number of neurons in each layer, and the number of outputs of the MLP may vary. If $K = N_{outputs}$, then a single MLP predicts all the desired output variables. If $K = 1$, then each output variable is predicted by its own MLP, and, hence, $N_{outputs}$ MLPs are required to predict all of the variables.

Each weight is assigned a numerical value, while each neuron has an associated activation function, again determined by the user, which can be non-linear. The neurons marked b are the bias neurons, which do not take an input from another neuron but instead are given a constant input of +1. During training, an input vector, \mathbf{r} , is presented to the MLP input neurons and is propagated to the first hidden layer according to

$$\mathbf{n}^1 = \text{act}^1(\mathbf{W}^1 \mathbf{r} + \mathbf{b}^1), \tag{4}$$

where \mathbf{n}^1 is the output from the first hidden layer, act^1 is the activation function for the first hidden layer, \mathbf{W}^1 is the matrix of weights connecting the neurons of the first hidden layer to those in the previous layer, and \mathbf{b}^1 is the vector of weights connecting the neurons in the first hidden layer to the bias neuron in the previous layer. This process is repeated through the remaining $l - 1$ hidden layers according to Eq. (5), until the MLP output, \mathbf{s}^* , is retrieved, as shown below:

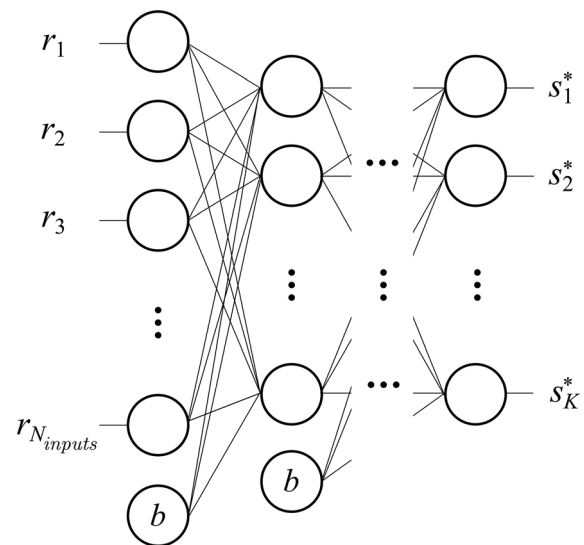


FIG. 1. Diagram of an MLP with K outputs showing neurons (circles) arranged in layers connected by weights (lines).

$$\mathbf{n}^l = \text{act}^l(\mathbf{W}^l \mathbf{n}^{l-1} + \mathbf{b}^l), \quad (5)$$

$$\mathbf{s}^* = \text{act}^{l+1}(\mathbf{W}^{l+1} \mathbf{n}^l + \mathbf{b}^{l+1}). \quad (6)$$

The errors between the MLP output and the target output for a given data point p are used to adjust the values of the weights of all layers, through a process known as backpropagation.⁴⁴ This adjustment aims to minimize a chosen loss function, L , over the training dataset, such as the mean squared error shown below:

$$L = \frac{1}{N_{data}} \sum_{p=1}^{N_{data}} \sum_{i=1}^K (s_i^p - s_i^{p,*})^2, \quad (7)$$

where N_{data} is the number of entries in the training dataset. Once the MLPs have been trained, they can be used to make predictions on new data.

If the predictions of the target outputs were perfect (i.e., $L = 0$), then the conservation laws would be automatically satisfied. As such, techniques that reduce the loss by increasing the MLP accuracy, such as the use of a single MLP for each species^{1,38} or the MMLP method,^{31,32} naturally reduce the error in the conservation laws. In practice, however, the amount of constraint violation will never be zero and some points may even severely violate the constraints in search of reduction in the loss function. To mitigate this, one possibility is to introduce a term to the loss function that penalizes constraint violation, as done, for example, in Bode *et al.*,⁴⁵ who included a penalty term for mass conservation. However, this does not guarantee that the constraints are not violated and furthermore raises the issue of how to weight each term in the loss function in order to effectively impose the penalty. Modifying the loss function is also problematic when using separate MLPs for each species, as the constraints contain sums over species which the separate MLPs have no knowledge of. In Sec. III, an algorithm will be proposed for satisfying conservation law constraints that does not suffer from these limitations.

III. AN ALGORITHM FOR SATISFYING CONSERVATION LAW CONSTRAINTS

In order to obey the conservation laws, the ANN predictions, \mathbf{s}^* , having been de-transformed to yield \mathbf{Y}^* , must satisfy certain constraints that consist of linear combinations of the species mass fractions. The first constraint is that the species mass fractions must be bounded,

$$0 \leq Y_i^*(t + \Delta t) \leq 1. \quad (8)$$

The mass conservation constraint is given by

$$\sum_{i=1}^{N_{sp}} Y_i^*(t + \Delta t) = 1. \quad (9)$$

The element conservation constraints are given by

$$\sum_{i=1}^{N_{sp}} A_{ji} Y_i^*(t + \Delta t) = Z_j(t), \quad (10)$$

where Z_j is the mass fraction of element j , and A_{ji} is the proportion of the mass of species i contributed by element j , with $j = 1, 2, \dots, N_e$ and N_e being the number of elements for which conservation is required in the reaction mechanism. Elements that do not participate

in reactions (such as nitrogen if present only as N_2 in a mechanism that does not include nitrogen chemistry) can be ignored. A composition that satisfies Eq. (10) will automatically satisfy Eq. (9), so to obey both mass and element conservation, it is sufficient to satisfy Eq. (10).

The basic procedure for correcting the ANN predictions in order to satisfy the conservation laws to machine precision will now be illustrated using a mixture consisting of only two species, with their mass fractions given by Y_1 and Y_2 . After the ANN predictions of both species are made, any negative predictions are set to zero and any mass fractions greater than one are clipped to satisfy Eq. (8). The aim is to obtain the mass fractions satisfying the conservation laws, Y_i^{con} . To start, Y_i^{con} are initialized to these bounded predictions. Then, in order to satisfy an element conservation constraint, a correction is applied to one of the predicted species mass fractions. For example, the value of Y_1 can be corrected,

$$Y_1^{con} = \frac{Z_j - A_{2j} Y_2^{con}}{A_{1j}}. \quad (11)$$

The composition will now satisfy the conservation law for the element being considered. Alternatively, the value of Y_2 can be corrected, with its new value obtained in a similar way using

$$Y_2^{con} = \frac{Z_j - A_{1j} Y_1^{con}}{A_{2j}}. \quad (12)$$

It should be noted that only one of Eq. (11) or Eq. (12) is needed in order to recalculate one species mass fraction to conserve the element under consideration. The species that is recalculated, thus, will be referred to as the residual species. It is only the mass fractions of the residual species that will be altered to satisfy the mass and element conservation laws with the mass fractions of the other species left unchanged.

To ensure that Y_i^{con} remains bounded, the recalculated residual species mass fractions must be also be bounded. In practice, the most common violation of the species mass fraction bounds occurs through negative mass fraction predictions. It is, therefore, worth examining how negative residual species mass fractions may arise. Looking at Eq. (11), the residual species mass fraction would be negative if the total amount of element contained in Y_2^{con} was predicted to be greater than the available amount of that element at time t . Figure 2 illustrates how a negative residual prediction could arise by arbitrary considering Y_1 as the residual species. From the top of Fig. 2, the first two horizontal bars show the contributions of each species to the element under consideration in the initial composition and the target composition, respectively. The third bar shows the contribution of each species to the element under consideration for fictitious ANN predictions. It can be seen in the third bar that there is a large overprediction in Y_2 compared to the target value and therefore a large overprediction of the amount of the element under consideration contained in Y_2 . In fact, the predicted amount of the element contained in Y_2 is larger than its total amount available at time t . In order to conserve this element, the value of Y_1 is, therefore, calculated via Eq. (11) to be negative. This is illustrated by the fourth bar in Fig. 2, where the total amount of the element is now conserved, but the contribution of Y_1 to the element is negative.

Figure 2 raises two important points for the foundations of the proposed method. The first is that the residual species should be

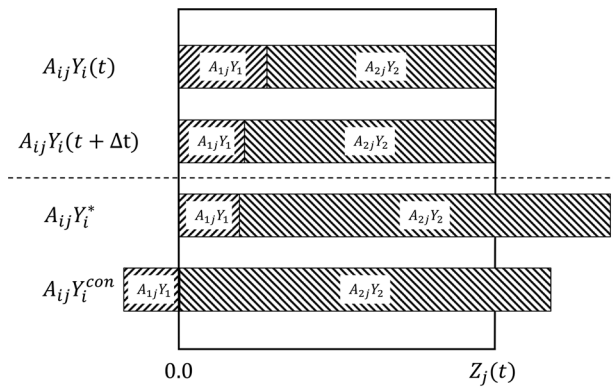


FIG. 2. Illustration of a large overprediction of Y_2^* resulting in a mass fraction of Y_1^{con} , which is calculated to be negative in order to satisfy the conservation law for the element under consideration.

chosen after the ANN predictions are made, and it should be the species that contains the highest possible amount of the element to be conserved in the predictions. This reduces the chance of the non-residual species containing more of the element than was available at time t and so reduces the chance of negative values being calculated for residual species. This has the important implication that the choice of residual species should be different for each composition. Figure 3 shows the same initial and target composition as Fig. 2, but now considers Y_2 as the residual species. Figure 3 shows that after using Eq. (12) the composition Y_i^{con} remains bounded. Because the contribution of Y_2^* to the element under consideration is so much larger than that of Y_1^* , the error in Y_1 would have to be extremely large to calculate Y_2^{con} as negative.

The second important point raised by Figs. 2 and 3 is that the chance of negative residual species mass fractions occurring will naturally decrease with increasing prediction accuracy, and so the method of recalculating residual species is complementary to approaches, which increase ANN accuracy. Wildly inaccurate predictions from a correctly implemented ANN method, such as those which are significantly out-of-bounds, are extremely uncommon and can be screened out. This

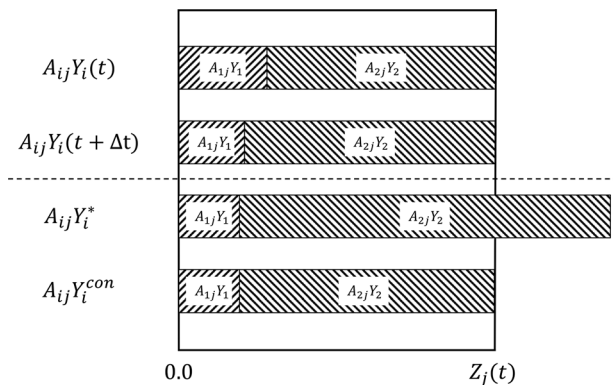


FIG. 3. Illustration of a large overprediction of Y_2^* , which can be corrected in order to satisfy the conservation law for the element under consideration by calculating Y_2^{con} .

screening-out could be performed, for example, by comparing the predicted value against the maximum value of the species found in the training set. A threshold can be set on the prediction value, above which the predictions are considered very inaccurate. Moderate prediction errors are easily absorbed by the proposed method.

The expansion of the method illustrated so far to a mixture containing an arbitrary number of species is straightforward. A separate residual species is chosen to satisfy each of the N_e element constraints. To proceed, it is simplest to eliminate the elements one at a time. For example, if the elements are C, H, and O, a possible choice of residual species is CH_4 (for C), H_2O (for H without changing C), and O_2 (for O without changing C or H). Another possibility is CH_4 (for C), H_2O (for H), and both of CO_2 and CO (for O without altering C). For simplicity, we restrict ourselves to using a single residual species for each element; hence, there are a total of N_e residual species. This has the consequence that the final residual species must contain a single element only to avoid disrupting the already conserved elements. This means the number of species that can be considered as the final residual species is limited, as is the number of possible orders in which to eliminate the elements.

Once the element solution order is determined, the first residual species is chosen as the species predicted to contribute the most to the mass fraction of the first element to be eliminated. The second residual species is the species that does not contain the first element and is predicted to contribute the most to the mass fraction of the second element. This process continues until all of the residual species have been determined. At that point, the residual species mass fractions can be recalculated to satisfy the mass and element conservation laws.

Depending on which species can be considered as the final residual species and the ANN accuracy, it may not be possible to avoid a negative final residual species. As an example, the GRI 1.2 mechanism has 31 species, but there are only six that contain a single element: H_2 , H, O, O_2 , C, and N_2 . The conservation of N is unnecessary in GRI 1.2, so N_2 is ignored. Of the remaining species, it is possible that none will occur in large enough amounts to prevent the error in the non-residual species from overwhelming the amount of the element under consideration at time t . Therefore, an algorithm is proposed to rectify a negative value in the final residual species, in the instances where it arises, without altering any of the other elements.

It may also be possible that, in the chosen mechanism, there are no species consisting of a single element only. While the method will be outlined in the simplest way possible by choosing a single residual species for each element, there is no reason why multiple residual species cannot be chosen to conserve the same element, in a similar spirit to the algorithm proposed as part of the method to rectify negative values of the final residual species mass fraction. This extension would increase the applicability of the method to even more mechanisms.

It should be noted at this point that the method does not depend on the choice of the time step, Δt , as only the element mass fractions at time t are used as reference for the conservation algorithm. Furthermore, unlike the conventional integration of ODEs that relies on the values of the dependent variables and their gradients at the current time, as well as on the time step, ANNs are trained using only initial and final value pairs, with the time step not entering at all the training process. If variable time step is required in a simulation, there are two ways of accommodating it. The first one is to have the ANNs trained for a minimal time step and call them in succession to make

ALGORITHM 1. Generate initial ANN prediction.

Require: $h(t), Y_i(t)$ ▷ Input composition
if ANNs predict outputs **then**
 $Y_i^*(t + \Delta t) = \text{ANNs}[h(t), Y_i(t)]$ ▷ Predicted outputs
else if ANNs predict changes **then**
 $\Delta Y_i^* = \text{ANNs}[h(t), Y_i(t)]$ ▷ Predicted changes
 $Y_i^*(t + \Delta t) = Y_i(t) + \Delta Y_i^*$ ▷ Predicted outputs
end if
for $i = 1, N_{sp}$ **do** ▷ Remove out of bounds predictions
if $Y_i^*(t + \Delta t) < 0$ **then**
 $Y_i^*(t + \Delta t) = 0$
end if
if $Y_i^*(t + \Delta t) > 1$ **then**
 $Y_i^*(t + \Delta t) = 1$
end if
end for
 $Y_i^b(t + \Delta t) = Y_i^*(t + \Delta t)$
return $Y_i^b(t + \Delta t)$ ▷ Bounded predictions

up integer multiples of it. The second one is to have more than one sets of ANNs, e.g., one trained with 10^{-6} s and one with 10^{-5} s, and use combinations of them.

This rest of this section details the computational implementation of the procedure for satisfying the conservation laws in ANNs, starting from the input composition, $[h(t), Y_i(t)]$, and finishing with a predicted composition, which is bounded and obeys the conservation laws, $Y_i^{com}(t + \Delta t)$. The procedure can be broken down into the following four steps:

1. Generate initial ANN predictions (Algorithm 1).
2. Select residual species (Algorithm 2).
3. Recalculate residual species mass fractions (Algorithm 3).
4. Rectify negative final residual species if necessary (Algorithm 4).

Each of these steps is described below. A worked example of the solution procedure using Algorithms 1–4 is also provided in the Appendix.

A. Step 1: Generate initial ANN predictions

The first step in the process is to generate the initial ANN predictions. If the ANNs predict the species, $Y_i^*(t + \Delta t)$, then these can be

ALGORITHM 2. Select residual species.

Require: $Y_i^b(t + \Delta t)$ ▷ Non-negative ANN predictions
Require: C_c ▷ Indices of N_c candidate final residuals
Require: E_c^C ▷ Indices of the elements contained in the candidates

Calculate predicted element mass fractions:
for $j = 1, N_e$ **do**
 $Z_j^b(t + \Delta t) = \sum_{i=1}^{N_{sp}} A_{ji} Y_i^b$
end for

Find the index of the final residual species in the candidates by calculating how much each candidate contributes to its element:
 $T = \text{maxloc} \left(\frac{1 \times Y_c^b}{Z_{E_c}^b} \right)$
 $S_{N_c} = C_T$ ▷ Index of final residual species in mechanism
 $E_{N_c} = E_T$ ▷ Index of element contained in final residual
 $E_j = (E_1, E_2, \dots, E_{N_c})$ ▷ Element solution order

Determine the other residual species:
for $k = 1, N_e - 1$ **do**
 Find indices of possible residual species for the current element, depending on the elements which have already been eliminated:
 $P_p = S_i^{tot}$ which contain E_k and may contain any of E_l , with $l = k + 1, N_e$
 Index of residual species for the k th element in the possible species:
 $T = \text{maxloc} \left(\frac{A_{E_k P_p} Y_{P_p}^b}{Z_{E_k}^b} \right)$
 Index of residual species for the k th element in the mechanism:
 $S_k = P_T$
end for
return S_p, E_j ▷ Indices of residual species and element solution order

ALGORITHM 3. Recalculate residual species mass fractions.

Require: $Y_i(t)$ ▷ Original species composition
Require: $Y_i^b(t + \Delta t)$ ▷ Bounded ANN predictions
Require: S_j ▷ Indices of residual species from Step 2
Require: E_j ▷ Element solution order from Step 2

Calculate element mass fractions at time t :
for $j = 1, N_e$ **do**
 $Z_j(t) = \sum_{i=1}^{N_{sp}} A_{ji} Y_i(t)$
end for
 $Y_i^{con}(t + \Delta t) = Y_i^b(t + \Delta t)$ ▷ Initialize conserved mass fractions
 $\beta_i = 1$ ▷ Set residual species switch
for $j = 1, N_e$ **do**
 $\beta_{S_j} = 0$ ▷ Set switch for current residual species
 Calculate element mass in all but the current residual species:
 $Z_{E_j}^{con} = \sum_{i=1}^{N_{sp}} \beta_i A_{E_j i} Y_i^{con}$
 Recalculate residual species mass fraction:
 $Y_{S_j}^{con} = \frac{Z_{E_j} - Z_{E_j}^{con}}{A_{E_j S_j}}$
 $\beta_{S_j} = 1$ ▷ Reset switch
if $Y_{S_j}^{con} < 0$ and $j \neq N_e$ **then**
 Go to Step 2 and try new element solution order.
end if
end for
return $Y_i^{con}(t + \Delta t)$ ▷ Composition obeying conservation laws

used directly. If the ANNs predict the changes in the species over a given time step, then predictions of the change, ΔY_i^* , can be made and added to the input composition to retrieve $Y_i^*(t + \Delta t)$. Any compositions with extremely unphysical predictions should be screened out. Any $Y_i^*(t + \Delta t)$ that lie moderately outside of the mass fraction bounds are set to lie within them, to give the bounded predictions $Y^b(t + \Delta t)$. If the ANNs predict $Y_i^*(t + \Delta t)$, then predictions can be guaranteed to be in bounds by using modified rectified linear unit (ReLU) activation functions on the output layer.

B. Step 2: Select residual species

The second step is to choose which of the predicted species to consider as residual species for the given composition. We have restricted ourselves to the final residual species, which are made up of a single element only. The number of candidate final residuals is denoted by N_C , while the index of each candidate final residual in the mechanism is stored in C_c . The index of the element contained in each of the candidate final residuals is denoted by E_c^C . Because the number of element solution orders is limited by the candidate final residuals, it is preferable to select the final residual species first in order to ensure that a valid order is chosen. To do this, the predicted element mass fractions are calculated using the bounded predictions. As explained previously, to try and avoid negative residual predictions, the final residual species, S_{N_e} , is chosen to be the candidate final residual species, which contributes the highest proportion of the mass of its

ALGORITHM 4. Rectify final residual species if needed.

Require: $Y_i^{con}(t + \Delta t)$ ▷ Conserved ANN predictions with negative final residual
Require: S_{N_e} ▷ Index of final residual species
Require: R_1, R_2 ▷ Indices of pairs of rectifying species for the final residual

Require: E^R ▷ Other element pair of rectifying species contain

$a = -A_{E_{N_e} S_{N_e}} Y_{S_{N_e}}^{con}$
 $b = A_{E_{N_e} R_1}$
 $c = A_{E_{N_e} R_2}$
 $d = \frac{A_{E^R R_1}}{A_{E^R R_2}}$
 $\Delta Y_{R_1}^{con} = \frac{-a}{b - cd}$ ▷ Change in first rectifying species mass fraction
 $\Delta Y_{R_2}^{con} = -d \Delta Y_{R_1}^{con}$ ▷ Change in second rectifying species mass fraction
 $Y_{R_1}^{con} = Y_{R_1}^{con} + \Delta Y_{R_1}^{con}$ ▷ New mass fraction of first rectifying species
 $Y_{R_2}^{con} = Y_{R_2}^{con} + \Delta Y_{R_2}^{con}$ ▷ New mass fraction of second rectifying species
 $Y_{S_{N_e}}^{con} = 0$ ▷ Negative final residual mass fraction zeroed
return $Y_i^{con}(t + \Delta t)$ ▷ Bounded conserved ANN predictions

respective element. The element solution order, E_j , for the N_e elements is, then, determined. The final element in the solution order, E_{N_e} , will be the one contained by the final residual species S_{N_e} . We have found the order for the remaining elements to be unimportant. Once the element solution order has been fixed, the remaining residual species can be determined. The residual species for the first element in the solution order is determined by finding the species, which contributes the most to the first element. The residual species for the second element is determined by finding the species, which contributes the most to the second element in the solution order but does not contain the first element. This continues until all but one element is eliminated (which is the element contained by the already determined final residual species).

C. Step 3: Recalculate mass fractions of residual species

Once the residual species have been determined, the correction to satisfy the conservation of mass and elements can be applied. The target element mass fractions, $Z_j(t)$, are calculated using the input composition. The conserved species mass fractions, $Y_i^{con}(t + \Delta t)$, are initialized to the bounded ANN predictions. A switch for the species, β_i , is introduced and set to one for all species. The switch for the first residual species, β_{S_1} , is set to zero. The predicted mass fraction of the first element to be conserved is calculated without the mass fraction of the first residual species, as follows:

$$Z_{E_1}^{con} = \sum_{i=1}^{N_{sp}} \beta_i A_{E_1 i} Y_i^{con}. \tag{13}$$

The mass fraction of the first residual species can then be recalculated in order to conserve the first element,

$$Y_{S_1}^{con} = \frac{Z_{E_1} - Z_{E_1}^{con}}{A_{E_1, S_1}}. \quad (14)$$

The switch for the first residual species, β_{S_1} , is then set to one again, and the process is repeated until all of the new residual species mass fractions are determined. The species mass fractions now conserve all of the elements, as well as the total mass. As explained in Sec. III, it is possible that a negative value may be encountered in the residual species, although this is unlikely owing to the choice of the choice of residual species as the one contributing the most to its corresponding element. If the residual species with the negative value is not the final one, a new solution order can be tried, and if negative residuals are still encountered, the composition can be rejected, while the new state can be calculated with direct integration. As long as such instances are rare, this will not impact on the time saving of the ANN tabulation. If a negative value in the final residual species is encountered, then it can be rectified using the algorithm to be described in step 4.

D. Step 4: Rectify final residual species if needed

If a negative value is encountered in the final residual species, it can be removed by modifying a pair of rectifying species, R_1 and R_2 , to make up for the required change in the final element without altering any of the other elements. For each candidate final residual species, a pair of rectifying species can be selected ahead of time from the species available in the mechanism. For a given candidate final residual, a pair of rectifying species must share one element other than the element contained in the respective candidate final residual, and (at least) one of the pair must contain the element contained in the respective candidate final residual. For example, if O_2 is chosen to be the final residual species, a possible pair of rectifying species is CO_2 and CO . Then, if the O_2 mass fraction is recalculated to be negative, its mass fraction can be set to zero. This introduces extra O element, which must be removed to satisfy element conservation. To do this, the mass fraction of CO_2 can be reduced and the mass fraction of CO increased to account for the O element without changing the C element. Alternatively, the rectifying species could have been chosen as H_2O and H_2 . It may be possible that a pair of rectifying species cannot be found for a given candidate final residual, in which case Algorithm 4 cannot be used directly if negative values are recalculated for that final residual. Algorithm 4 shows how a negative value in the mass fraction of the final residual species can be rectified.

After using Algorithms 1–3, and Algorithm 4 if necessary, the predicted composition now satisfies the bounds and the conservation laws. A worked example of the method is given in the Appendix. Section IV applies this conservation method to one-dimensional premixed flame simulations to evaluate its effectiveness.

IV. APPLICATION TO ONE-DIMENSIONAL PREMIXED FLAMES

A. Simulation methodology

In the present section, reaction source term computations in simulations of one-dimensional adiabatic premixed flames are performed with three approaches: direct integration (DI) with the VODE solver,⁴⁶ ANNs, and ANNs with the conservation method proposed here.

The complete set of the equations describing the one-dimensional premixed flames simulated here can be found in Ref. 47. Here, we focus on the species transport equation, which can be written as follows:

$$\rho \frac{\partial Y_i}{\partial t} + \frac{\partial \rho(u + V_c)Y_i}{\partial x} = \frac{\partial}{\partial x} \left(\rho D_i \frac{W_i}{W} \frac{\partial X_i}{\partial x} \right) + \dot{\omega}_i, \quad (15)$$

where u is the velocity, x is the spatial position, ρ is the density, D_i is the diffusivity, W_i is the molecular weight of species i , W is the mean molecular weight, X_i is the mole fraction, and $\dot{\omega}_i$ is the reaction source term. V_c is a correction velocity introduced to satisfy mass conservation and is given by

$$V_c = \sum_{i=1}^{N_{sp}} D_i \frac{W_i}{W} \frac{\partial X_i}{\partial x}. \quad (16)$$

To simulate the flames, Eqs. (15) and (16) are discretized and solved with the method of fractional steps. With this formulation, the reaction source term is solved within its own fractional step as a system of ODEs of the following form:

$$\dot{\omega}_i = \frac{dY_i}{dt} = f(h, Y_i). \quad (17)$$

These ODEs are solved as an initial value problem using either DI or the ANNs with or without conservation. This yields a mapping of the form of Eq. (1) and so is well suited for the proposed conservation methodology. Details of the simulations are given in Table I. The domain was filled with fuel/air mixture at the chosen equivalence ratio. To ignite the flame, half of the domain was initialized to equilibrium conditions, while the other half was initialized as unburnt. A minimum temperature of 500 K was set for a point in the domain to be considered reactive.

Two flames are computed: a CH_4 -air flame, computed with the GRI 1.2⁴² mechanism, and a C_3H_8 -air flame, computed with the USC Mech II mechanism.⁴³ GRI 1.2 contains thirty one species and four elements (C, H, O, and N), while USC Mech II contains 111 species and five elements (C, H, O, N, and Ar). However, neither mechanism includes nitrogen chemistry, with N_2 being the only species including N, while Ar is inert and neglected. Therefore, in simulations with either mechanism, there are constraints only for three elements, namely, C, H, and O, as well as the constraint that the reacting species mass fractions must sum to $1 - Y_{N_2}(t)$. There are five candidate final residual species for both mechanisms, which were identified as C, H_2 , H, O, and O_2 . For H_2 and H, the rectifying species were chosen to be H_2O and OH, while for O_2 and O, they were CO_2 and CO. Although it is very unlikely that C will ever be used as the final residual species due to its general small contribution to the C element, its rectifying

TABLE I. Premixed flame simulation details.

Domain length	10 mm
Grid nodes	600
Unburnt temperature	300 K
Time step	1 μ s
Simulation length	0.02 s

TABLE II. GRI 1.2 training set information and ANN architecture.

Parameter	Value
ϕ range	0.45–1.70
Number of data	370 000
Targets	$Y_i(t + \Delta t)$
Number of layers	4
Neurons per layer	32-30-30-1
Scaling	Linear to $(-1, 1)$
Activation functions	n/a - tanh(x) - tanh(x) - max(-1, x)
Training method	Levenberg–Marquardt ⁴⁸ with Bayesian regularization ⁴⁴
Number of training iterations	1500

species are chosen as CO₂ and O₂. Finally, non-equal diffusivities are used for both flames.

To construct the training sets for the ANNs, composition states were sampled randomly throughout one-dimensional premixed flame simulations with equal diffusivities at varying equivalence ratios using the same method and parameters as in Table I. These composition states were used as a basis for random data generation following the method shown in Ding *et al.*^{31,32} and Readshaw *et al.*,¹ before being discarded. The randomly generated data were then integrated using VODE over a time step $\Delta t = 1 \mu\text{s}$ to form the input/target pairs of the ANN training data sets. Single output MLPs were used for each species, and the training set and ANN architecture information are shown in Table II for the GRI 1.2 mechanism ANNs and Table III for the USC Mech II ANNs. Linear scaling on the inputs and the outputs was performed using the minimum and maximum values of the respective quantities in the training set. Note also that we have chosen $Y_i(t + \Delta t)$ and ΔY_i as targets for GRI 1.2 and USC Mech II, respectively, with different output activation functions for each in order to demonstrate the applicability of the proposed method to a range of activation functions and outputs.

While the MMLP machine learning methodology has been demonstrated before to yield good predictions in a range of problems including laminar flamelets, one-dimensional laminar premixed flames, and turbulent flames with pure fuels and fuel blends,^{1,31,32}

TABLE III. USC Mech II training set information and ANN architecture.

Parameter	Value
ϕ range	0.50–2.50
Number of data	250 000
Targets	ΔY_i
Number of layers	4
Neurons per layer	112-20-20-1
Scaling	Linear to $(-1, 1)$
Activation functions	n/a - tanh(x) - tanh(x) - x
Training method	Levenberg–Marquardt ⁴⁸ with Bayesian regularization ⁴⁴
Number of training iterations	1000

all without using data from the training problem, in the present paper, we concentrate on the improvement afforded by the conservation algorithm, and hence, only one-dimensional laminar premixed flames are simulated. However, the test case chosen is the simulation of one-dimensional premixed flames with non-equal diffusivities, while training was performed on data originating from one-dimensional premixed flames with equal diffusivities. This difference introduces an additional challenge to the ANNs and will, therefore, allow the difference in accuracy between ANNs with and without conservation to be more readily highlighted. It should also be noted, however, that in general one-dimensional premixed flames still present a stiff challenge to the machine learning tabulation approach. The training dataset is generated with the hybrid premixed flame—random data method outlined above, with the initial data collected from premixed flames discarded. Furthermore, the ANNs are trained to predict the reaction outcome at single composition states and are oblivious to the structure of premixed flames. Finally, the simulation of the premixed flames with ANNs is performed with an unsteady method where the premixed flame structure is allowed to evolve to a steady state. As such, the simulation is subject to accumulation of errors that pose a very stringent test to the ANN-tabulated kinetics, whose mitigation is the objective of the proposed methodology.

B. CH₄-air flames (GRI 1.2)

Table IV shows the root mean square error (RMSE) in each of the quantities that should be conserved over all of the reacting points throughout simulations with non-equal diffusivities at $\phi = 1.0$ for GRI 1.2, when using the ANNs with and without conservation. It can be seen that the ANN predictions are subject to an error in the conserved quantities. Although this error is small, it can accumulate as a simulation progresses. In contrast, constraining the ANN predictions using Algorithms 1–4 shows that all of the quantities are conserved to machine precision for every single reacting point. Results are only shown for $\phi = 1.0$, but the application of conservation has the same effect in the other cases as well.

Figures 4 and 5 show the steady-state CO and H₂ mass fraction profiles for the CH₄-air flames as computed with the three aforementioned integration methods. The specific species profiles have been selected for display as these species are generally more difficult to predict than other major species; furthermore, they are often chosen as residual species; hence, their predictions would highlight any adverse effects of incorporating the conservation laws on predictions of residual species. It should also be mentioned that the machine learning tabulation methodology employed here has been shown before to yield good results for both major and minor species in laminar premixed

TABLE IV. Root mean square error in conserved quantities across the reaction step over all reacting points throughout simulations with non-equal diffusivities at $\phi = 1.0$ and GRI 1.2.

Quantity	ANNs RMSE	ANNs with conservation RMSE
Y_O^e	1.97×10^{-7}	1.51×10^{-18}
Y_H^e	6.91×10^{-7}	1.75×10^{-18}
Y_C^e	1.39×10^{-7}	3.57×10^{-19}
$1 - Y_{N_2}$	2.38×10^{-9}	3.60×10^{-20}

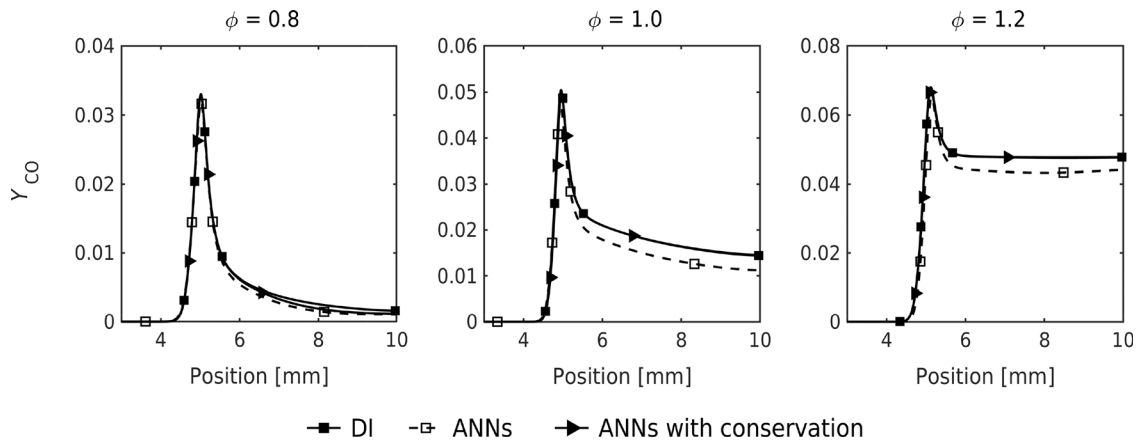


FIG. 4. CO mass fraction profiles at the end of GRI 1.2 one-dimensional premixed flame simulations with non-equal diffusivities when using different methods for reaction source term integration.

flames, as well as in flamelets and turbulent flames;^{1,31,32} hence, there is no need to show the profiles of all species. It can be seen that the application of conservation has a positive effect on the overall accuracy of the simulations using ANNs, with barely perceptible differences between the DI profiles and those of the ANNs with conservation. Ding *et al.*³¹ showed similarly excellent agreement in one-dimensional premixed flames by using the MMLP method to increase ANN prediction accuracy. Here, however, a simpler ANN architecture has been used to achieve the same accuracy. Using a simpler ANN architecture leads to smaller inference times and, therefore, simpler ANNs, which incorporate that the conservation laws can be used to obtain the same accuracy as more complex ANNs, which do not, thus providing greater speed-up in reacting flow simulations. Alternatively, the improved accuracy owing to the conservation scheme can add up to that of the MMLP method, for the benefit of increased accuracy in future turbulent reacting flow simulations.

Figures 6 and 7 show the steady-state molar H/C and O/N profiles. Significant differences in the profiles can be seen when comparing the ANNs without conservation to the DI profiles. On the other

hand, the ANNs with conservation are much closer in agreement with the DI profiles. The action of differential diffusion means that even if element conservation is absolutely satisfied during the reaction fractional step, a small difference can still be expected between DI and ANNs due to the diffusion step. Nevertheless, it is clear that as well as ensuring physical consistency, satisfying the conservation laws also improves ANN predictive accuracy in applications by reducing the accumulation of element errors, which feed into input species mass fractions for the following time steps.

Table V gives the percentage frequency of different residual species permutations recorded throughout one-dimensional premixed flame simulations with non-equal diffusivities for GRI 1.2 at different equivalence ratios. It can be noted that, at fuel lean and stoichiometric equivalence ratios, the most commonly used permutation is (CO₂, H₂O, O₂), and, furthermore, there are no instances of permutations using H₂ as the final residual species. At $\phi = 1.2$, the permutation (CO₂, H₂O, and H₂) becomes the most common as there is less O₂ available, while at $\phi = 1.4$, there is not enough O₂ to produce large amounts of CO₂ and so (CO, H₂O, and H₂) is the most common

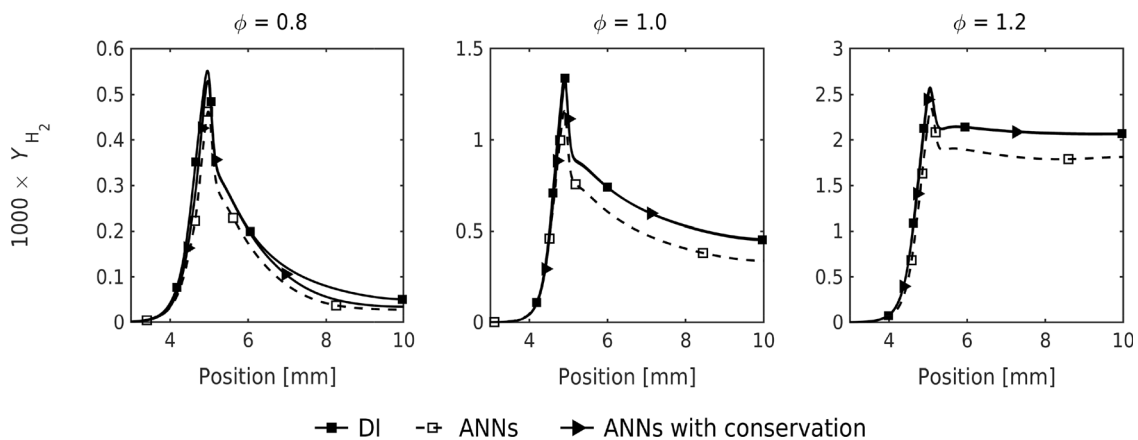


FIG. 5. H₂ mass fraction profiles at the end of GRI 1.2 one-dimensional premixed flame simulations with non-equal diffusivities when using different methods for reaction source term integration.

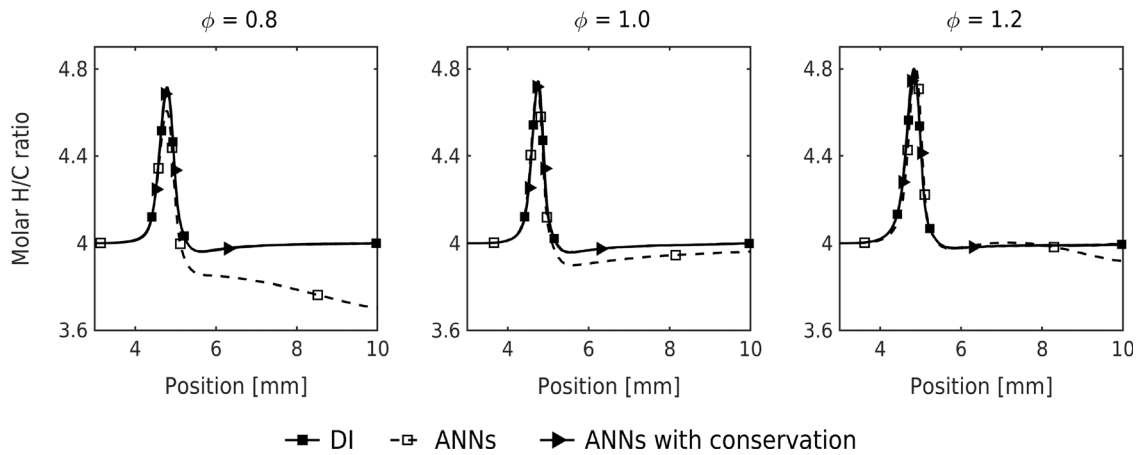


FIG. 6. Molar H/C ratio profiles at the end of GRI 1.2 one-dimensional premixed flame simulations with non-equal diffusivities when using different methods for reaction source term integration.

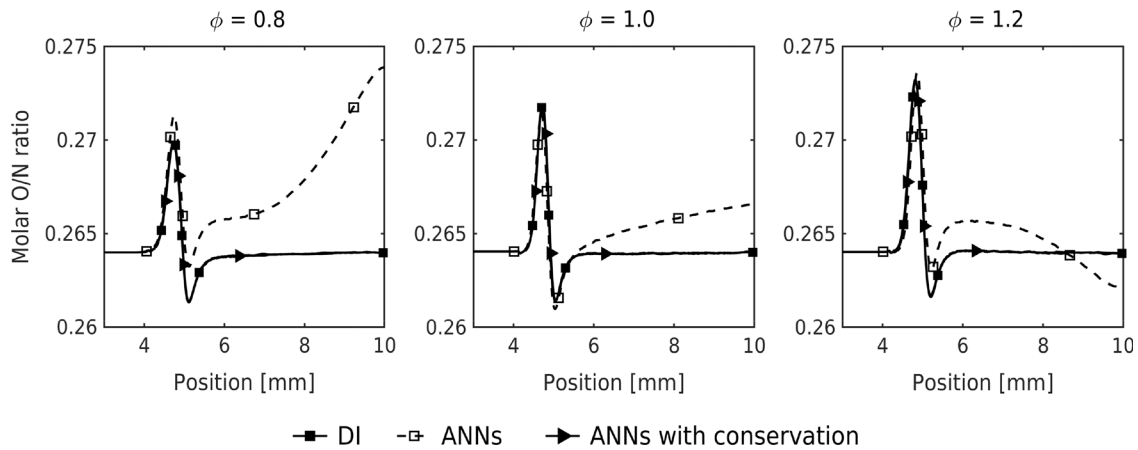


FIG. 7. Molar O/N ratio profiles at the end of GRI 1.2 one-dimensional premixed flame simulations with non-equal diffusivities when using different methods for reaction source term integration.

TABLE V. Percentage frequency of residual species permutations at different equivalence ratios for one-dimensional premixed flames with non-equal diffusivities and GRI 1.2.

Permutation	Percentage frequency (%)				
	$\phi = 0.6$	$\phi = 0.8$	$\phi = 1.0$	$\phi = 1.2$	$\phi = 1.4$
CH ₄ H ₂ O O ₂	9.4	10.0	8.2	10.3	18.3
CO H ₂ O O ₂	11.1	3.8	6.5	5.1	5.1
CO H ₂ O H ₂	8.1	76.6
CO ₂ H ₂ O O ₂	79.4	86.2	85.3	0.2	...
CO ₂ H ₂ O H ₂	76.3	...
C ₂ H ₂ H ₂ O O ₂	0.1

permutation. As expected, there are no instances of C being used as a final residual species due to its very low mass fraction.

Table VI shows the average central processing unit (CPU) time required to perform reaction step calculations in the one-dimensional

TABLE VI. Average time taken to perform one reaction step in GRI 1.2 one-dimensional premixed flame simulations with non-equal diffusivities at $\phi = 1.0$ with each integration method using a single Intel Xeon 6132 2.6 GHz CPU.

Method	CPU time (s)	Speed-up
DI	0.7228	...
ANNs	0.0245	30×
ANNs with conservation	0.0251	29×

TABLE VII. Root mean square error in conserved quantities across the reaction step over all reacting points throughout simulations with non-equal diffusivities at $\phi = 1.0$ for USC Mech II.

Quantity	ANNs RMSE	ANNs with conservation RMSE
Y_O^e	5.74×10^{-7}	1.99×10^{-18}
Y_H^e	8.08×10^{-6}	3.35×10^{-18}
Y_C^e	3.06×10^{-7}	9.60×10^{-19}
$1 - Y_{N_2}$	4.95×10^{-9}	8.65×10^{-20}

premixed flame simulations with each integration method for the GRI 1.2 mechanism. For GRI 1.2, reaction step calculations in the one-dimensional premixed flames with ANNs are on average 30× faster than using the VODE solver. Employing the correction for the conservation laws incurs a negligible computational cost compared to the ANN inference time and remains on average 29× faster than the VODE solver.

C. C₃H₈-air flames (USC Mech II)

Table VII shows the root mean square error in each of the quantities that should be conserved over all of the reacting points throughout simulations with non-equal diffusivities at $\phi = 1.0$ for USC Mech II when using the ANNs with and without conservation. As in the case of the CH₄-air flame, the conservation laws are satisfied to machine precision for every reacting point throughout simulations at any equivalence ratio.

Figures 8 and 9 show the steady-state CO and H₂ mass fraction profiles for the C₃H₈-air flames with the three different integration methods. USC Mech II is a more complex mechanism than GRI 1.2; hence, the accuracy of the ANNs both with and without conservation is lower, but it can still be seen that satisfying the conservation laws on the ANNs has a positive effect on their accuracy, leading to profiles, which agree more closely with the DI profiles. This is particularly evident in Figs. 8 and 9 at $\phi = 0.75$, where the profiles for the ANNs without conservation are obviously different from the DI profiles, while the

ones for the ANNs with conservation capture the peak location and general shape of the profiles with a much higher degree of accuracy.

Figures 10 and 11 show the steady-state molar H/C and O/N profiles. As before, a difference can be seen even between the ANNs with conservation and the DI profiles due to the differential diffusion, and it is more pronounced here because the difference in the species profiles is more noticeable, particularly at $\phi = 0.75$. However, it can still be seen that satisfying the conservation laws prevents the more unphysical deviations from the DI composition space, for example, as seen in the O/N profile at $\phi = 1.5$.

Table VIII gives the percentage frequency of different residual species permutations arising throughout the C₃H₈-air flame simulations. The use of USC Mech II results in more permutations than in the case of GRI 1.2, although the species involved are similar in both cases. Again, the automatic switch from the permutation of (CO₂, H₂O, O₂) to (CO, H₂O, H₂) can be seen as the initial mixture moves from fuel lean to fuel rich.

Table IX shows the average CPU time required to perform reaction step calculations in the one-dimensional premixed flame simulations with each integration method for the USC Mech II mechanism. The USC Mech II mechanism is more complex than GRI 1.2 so the speed-up when using ANNs is larger: On average, it is 56× faster when using ANNs compared to the VODE solver. Once again, the time needed to apply the conservation correction is very small compared to the ANN inference time, and the reaction source term computations using ANNs with conservation are still 54× faster than those with the VODE solver. The results from this section show that applying the conservation laws to the ANN predictions gives significant accuracy benefits with very little additional computational cost.

V. CONCLUSIONS

A method of satisfying element and mass conservation laws when using ANNs for the integration of reaction source terms has been developed. Certain species in a given reaction mechanism are selected as residual species, and the mass fractions of these species are recalculated after all of the ANN predictions are made in order to satisfy the conservation laws to machine precision. An automatic procedure for determining which species should be chosen as residual

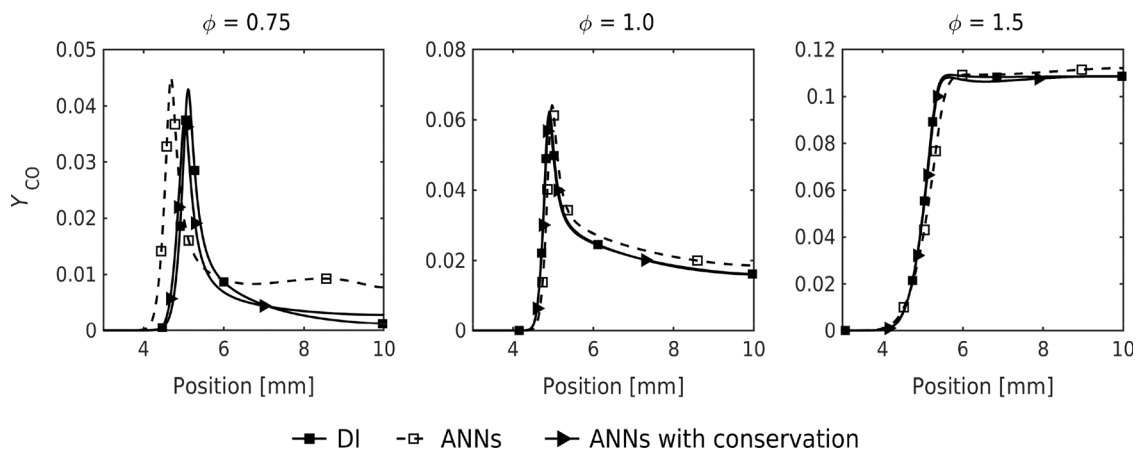


FIG. 8. CO mass fraction profiles at the end of USC Mech II one-dimensional premixed flame simulations with non-equal diffusivities when using different methods for reaction source term integration.

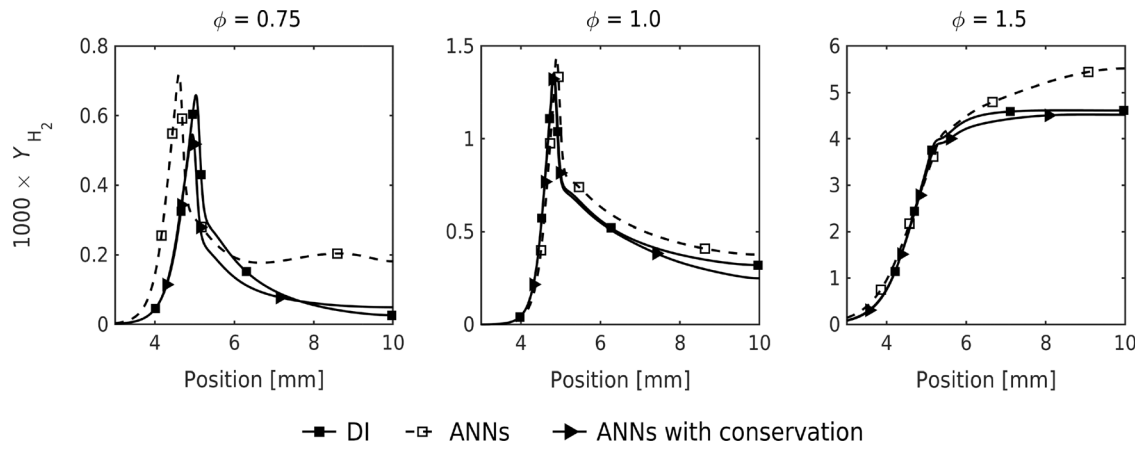


FIG. 9. H_2 mass fraction profiles at the end of USC Mech II one-dimensional premixed flame simulations with non-equal diffusivities when using different methods for reaction source term integration.

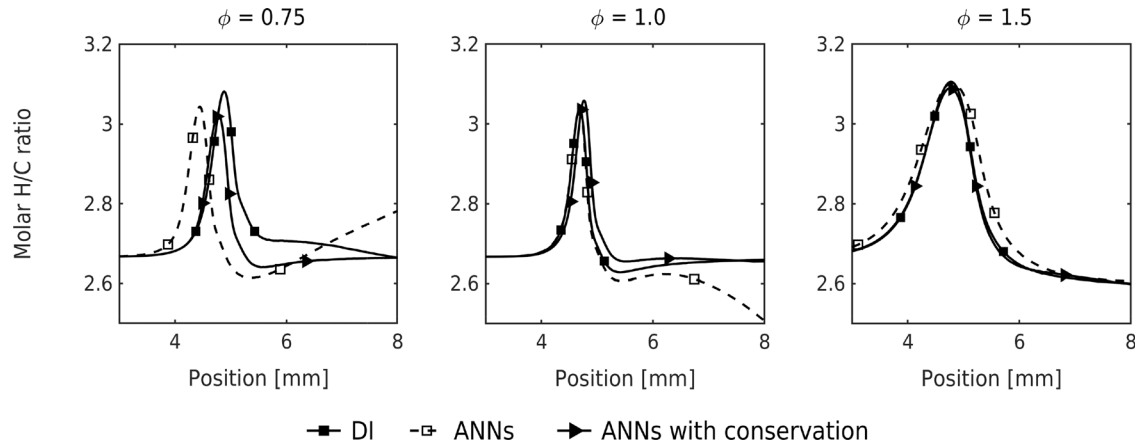


FIG. 10. Molar H/C ratio profiles at the end of USC Mech II one-dimensional premixed flame simulations with non-equal diffusivities when using different methods for reaction source term integration.

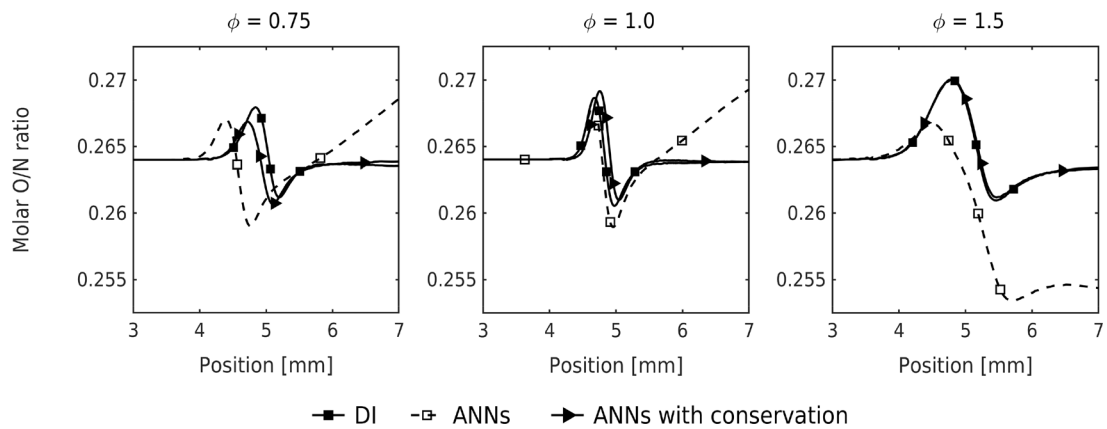


FIG. 11. Molar O/N ratio profiles at the end of USC Mech II one-dimensional premixed flame simulations with non-equal diffusivities when using different methods for reaction source term integration.

18 July 2023 09:12:53

TABLE VIII. Percentage frequency of residual species permutations at different equivalence ratios for one-dimensional premixed flames with non-equal diffusivities and USC Mech II.

Permutation	Percentage frequency (%)					
	$\phi = 0.7$	$\phi = 1.0$	$\phi = 1.5$	$\phi = 2.0$	$\phi = 2.5$	
C ₃ H ₈ H ₂ O O ₂	2.6	0.3	1.3	9.2	...	
C ₃ H ₈ H ₂ O ₂	3.4	...	
C ₃ H ₈ O ₂ H ₂	1.5	
CO H ₂ O O ₂	3.7	7.2	6.1	5.8	...	
CO H ₂ O ₂	0.8	...	
CO H ₂ O H ₂	92.6	71.2	78.2	
CO O ₂ H ₂	9.5	20.3	
CO ₂ H ₂ O O ₂	93.7	89.5	
CO ₂ H ₂ O H ₂	...	3.0	

TABLE IX. Average time taken to perform one reaction step in USC Mech II one-dimensional premixed flame simulations with non-equal diffusivities at $\phi = 1.0$ with each integration method using a single Intel Xeon 6132 2.6 GHz CPU.

Method	CPU time (s)	speed-up
DI	5.924	...
ANNs	0.106	56×
ANNs with conservation	0.110	54×

species for a given composition has been detailed, which increases the robustness of the method and removes the need for heuristics to inform the residual species selection. Species mass fraction predictions are set to be bounded between zero and one. The method is formulated so that negative predictions of residual species can be avoided in almost all cases. Furthermore, an algorithm is provided for rectifying negative values in the residual species in the rare cases where they may occur.

The proposed method can be readily adapted to any reacting system and can be easily combined with the existing ANN architectures for methods that involve direct coupling of chemistry and flow. These methods include transported probability density function (PDF) methods, direct numerical simulation (DNS), conditional moment closure (CMC), unsteady flamelet, multiple mapping closure (MMC), thickened flame model, linear eddy model (LEM), and partially stirred reactor (PaSR) as in OpenFOAM and laminar flame computations.

The method has been applied to two sets of one-dimensional premixed flame simulations: CH₄-air flames with the GRI 1.2 mechanism and C₃H₈-air flames with the USC Mech II mechanism. The results showed that the use of ANNs without conservation introduces small errors in the conserved quantities, and these errors accumulate throughout the simulation. In contrast, the ANNs with conservation satisfy the element and mass conservation laws for every reacting point to machine precision. Element ratio and species profiles from the ANNs with conservation were in very good agreement with the DI profiles, while considerable improvement was observed for the ANNs with conservation. This shows that, as well as guaranteeing physical consistency, satisfying the conservation laws positively impacts the accuracy of simulations.

At no point in any of the simulations (for GRI 1.2 or USC Mech II) were any ANN predictions screened out and DI used, nor were any negative residual species predicted, and therefore, in this case, Algorithm 4 was never required. This shows that, given sufficient ANN accuracy and the sensible selection of residual species by the proposed algorithm, the chance of predicting negative residual species is small. However, it is still theoretically possible to encounter negative residual species, depending on the ANN accuracy. Therefore, the strategy to remove the negative final residual prediction in Algorithm 4 should still be incorporated as part of the solution scheme.

The time taken to perform the simulations shows that the reaction source term computations with both ANN methods are significantly faster than using DI, with the speed-up factor in the case of USC Mech II reaching 56× and 54× for ANNs without and with conservation, respectively. The extra time required by augmenting of the ANNs with the conservation procedure is very small, and, therefore, the extra accuracy comes at a very low computational cost. Future work will exploit the method in the context of turbulent flame simulations with ANN-tabulated thermochemistry.

ACKNOWLEDGMENTS

Thomas Readshaw gratefully acknowledges the support by the Engineering and Physical Sciences Research Council (EPSRC) and Rolls-Royce plc in the form of a Doctoral Training Partnership (DTP) and Cooperative Award in Science and Technology (CASE) award. Thomas Readshaw would also like to thank Tianjie Ding for his helpful feedback on early versions of the paper.

AUTHOR DECLARATIONS

Conflict of Interest

The authors have no conflicts to disclose.

Author Contributions

Thomas Readshaw: Conceptualization (lead); Data curation (lead); Formal analysis (lead); Methodology (lead); Software (lead); Validation (lead); Visualization (lead); Writing – original draft (lead); Writing – review & editing (equal). **William Philip Jones:** Software (supporting); Supervision (supporting); Writing – original draft (supporting); Writing – review & editing (supporting). **Stelios Rigopoulos:** Conceptualization (supporting); Formal analysis (supporting); Funding acquisition (lead); Investigation (supporting); Methodology (supporting); Project administration (lead); Resources (lead); Software (supporting); Supervision (lead); Writing – original draft (supporting); Writing – review & editing (equal).

DATA AVAILABILITY

The data that support the findings of this study are available from the corresponding author upon reasonable request.

APPENDIX: EXAMPLE OF APPLICATION OF THE PROCEDURE FOR SATISFYING CONSERVATION LAWS IN THE ANN PREDICTIONS

Here, we demonstrate the procedure proposed in the present paper via an example of methane combustion with the seven-

TABLE X. Elements and species contained in the mechanism and their respective indices.

Index	Element	Index	Species
1	C	1	CH ₄
2	H	2	O ₂
3	O	3	CO
4	N	4	CO ₂
		5	H ₂
		6	H ₂ O
		7	N ₂

species four-step mechanism of Jones and Lindstedt.⁴⁹ This mechanism consists of the elements C, O, H, and N, and contains the species CH₄, O₂, CO, CO₂, H₂, H₂O, and N₂ with the indices given in Table X. It should be noted that no ANN predictions were actually carried out. Instead, an artificial initial set of values was constructed for the sake of the demonstration, so as to incur a significant conservation error that will be remedied by the proposed algorithm. In practice, a good ANN procedure would not incur so severe conservation errors in the first place. Furthermore, the fictitious composition has been chosen so that the procedure calculates a negative value in a residual species, so that the use of Algorithm 4 can also be demonstrated, although this did not occur in the cases shown in the paper due to the accuracy in the ANN predictions.

In this mechanism, N₂ is inert and is the only nitrogen containing species, meaning it is not necessary to approximate it with ANNs or to satisfy conservation of the N element. This means that N_e = 3. The candidate final residual species are those, which only contain a single element, hence O₂ and H₂, meaning that N_C = 2, C_c = (2, 5), and E_c^C = (3, 2). The rectifying species for O₂ are CO₂ and CO, meaning that R₁ = 4, R₂ = 3, and E^R = 1. In this mechanism, there are no pairs of rectifying species available for H₂ and, therefore, although it can be used as a final residual if calculated to be negative, the composition should be recalculated with O₂ used as the final residual instead.

1. Generate initial ANN predictions

Column 2 of Table XI gives an example input composition. Following Algorithm 1, the required ANN predictions should be carried out although, as mentioned, we have generated fictitious predictions for the purpose of illustration. These fictitious predictions are

TABLE XI. Mass fractions of species at various stages in Algorithm 1.

Species	Y _i (t)	Y _i [*] (t + Δt)	Y _i ^b (t + Δt)
CH ₄	0.011	0.008	0.008
O ₂	0.031	0.081	0.081
CO	0.045	0.025	0.025
CO ₂	0.141	0.143	0.143
H ₂	0.007	0.006	0.006
H ₂ O	0.147	0.148	0.148
N ₂	(0.618)	(0.618)	(0.618)

shown in column 3 of Table XI. Any unbounded predictions in Y_i^{*}(t + Δt) are returned within bounds, giving column 4 of Table XI.

2. Select residual species

The next step is to use Algorithm 2 to select the residual species. The predicted element mass fractions are calculated and shown in Table XII.

Then, the predicted contribution of each candidate final residual species to its respective element is calculated. For the first candidate final residual (O₂),

$$\frac{Y_{C_1}^b}{Z_{E_1^C}^b} = \frac{Y_2^b}{Z_3^b} = \frac{0.0810}{0.3307} = 0.2449.$$

For the second candidate final residual (H₂),

$$\frac{Y_{C_2}^b}{Z_{E_2^C}^b} = \frac{Y_5^b}{Z_2^b} = \frac{0.0060}{0.0246} = 0.2442.$$

For this composition, O₂ is predicted to contribute the most to its respective element mass fraction, so T = 1 and S_{N_c} = C₁ = 2. This means that the final element in the solution order is O, as E_{N_c} = E₁^C = 3. The rest of the element solution order is unimportant and is chosen as E₁ = 1 and E₂ = 2 to give the element solution order as E_j = (1, 2, 3) or (C, H, O). The remaining residual species are now determined. The possible species from which the first residual species is determined are

$$P_p = S_i, \text{ which contain } E_1 \text{ and may contain } E_2 \text{ and / or } E_3,$$

which are P_p = (1, 3, 4) or (CH₄, CO, CO₂). The contributions of each of these species to element E₁ are now calculated. For CH₄,

$$\frac{A_{E_1 P_1} Y_{P_1}^b}{Z_{E_1}^b} = \frac{A_{11} Y_1^b}{Z_1^b} = \frac{0.7487 \times 0.0080}{0.0557} = 0.1075,$$

for CO,

$$\frac{A_{E_1 P_2} Y_{P_2}^b}{Z_{E_1}^b} = \frac{A_{13} Y_3^b}{Z_1^b} = \frac{0.4288 \times 0.0250}{0.0557} = 0.1923,$$

and for CO₂,

$$\frac{A_{E_1 P_3} Y_{P_3}^b}{Z_{E_1}^b} = \frac{A_{14} Y_4^b}{Z_1^b} = \frac{0.2729 \times 0.1430}{0.0557} = 0.7002.$$

TABLE XII. Target and predicted element mass fractions, calculated from species in Table XI.

Quantity	Y _i (t)	Y _i ^b (t + Δt)
$\sum_{i=1}^{N_{sp}} Y_i$	1.0000	1.0290
Z _C	0.0660	0.0557
Z _H	0.0262	0.0246
Z _O	0.2898	0.3307
Z _N	(0.6180)	(0.6180)

18 July 2023 09:12:53

Therefore, $T = 3$ and $S_1 = P_T = P_3 = 4$, meaning that CO_2 is the first residual species. For the second residual species,

$$P_p = S_i, \quad \text{which contain } E_2 \text{ and may contain } E_3,$$

so the possible residual species for the second element are $P_p = (5, 6)$ or $(\text{H}_2, \text{H}_2\text{O})$. The contributions of the possible residual species for E_2 to the mass fraction of E_2 are now calculated. For H_2 ,

$$\frac{A_{E_2 P_1} Y_{P_1}^b}{Z_{E_2}^b} = \frac{A_{25} Y_5^b}{Z_2^b} = \frac{1.0000 \times 0.0060}{0.0246} = 0.2442,$$

and for H_2O ,

$$\frac{A_{E_2 P_2} Y_{P_2}^b}{Z_{E_2}^b} = \frac{A_{26} Y_6^b}{Z_2^b} = \frac{0.1119 \times 0.148}{0.0246} = 0.6740.$$

Therefore, $T = 2$ and $S_2 = P_T = P_2 = 6$, meaning that H_2O is the second residual species. As the final residual species has already been determined, all of the residual species are now determined and are $S_j = (4, 6, 2)$ or $(\text{CO}_2, \text{H}_2\text{O}, \text{O}_2)$.

3. Recalculate mass fractions of residual species

With the residual species determined, Algorithm 3 is now used to recalculate the mass fractions of the residual species in order to make the overall composition satisfy element and mass conservation. The target element mass fractions are calculated and shown in Table XII. The conserved mass fractions are initialized to the non-negative mass fractions from step 1. The residual species mass fractions are recalculated in turn using

$$Y_{S_j}^{\text{con}} = \frac{Z_{E_j} - \sum_{i=1}^{N_{sp}} \beta_i A_{E_j i} Y_i^{\text{con}}}{A_{E_j S_j}}.$$

The mask β_i is set to one for all species. Then, to recalculate the mass fraction of the first residual species, β_{S_1} is set to zero, i.e., $\beta_4 = 0$. For the first residual species,

$$Y_{S_1}^{\text{con}} = \frac{Z_{E_1} - \sum_{i=1}^{N_{sp}} \beta_i A_{E_1 i} Y_i^{\text{con}}}{A_{E_1 S_1}} = \frac{Z_1 - \sum_{i=1}^{N_{sp}} \beta_i A_{1i} Y_i^{\text{con}}}{A_{14}} = 0.1807.$$

Next, β_{S_1} is set to one, and then, β_{S_2} is set to zero: $\beta_4 = 1$ and $\beta_6 = 0$. The mass fraction of the second residual species is recalculated as follows:

$$Y_{S_2}^{\text{con}} = \frac{Z_{E_2} - \sum_{i=1}^{N_{sp}} \beta_i A_{E_2 i} Y_i^{\text{con}}}{A_{E_2 S_2}} = \frac{Z_2 - \sum_{i=1}^{N_{sp}} \beta_i A_{2i} Y_i^{\text{con}}}{A_{26}} = 0.1627.$$

Finally, β_{S_2} is set to one, while β_{S_3} is set to zero: $\beta_6 = 1$ and $\beta_2 = 0$. The mass fraction of the final residual species is recalculated as follows:

$$Y_{S_3}^{\text{con}} = \frac{Z_{E_3} - \sum_{i=1}^{N_{sp}} \beta_i A_{E_3 i} Y_i^{\text{con}}}{A_{E_3 S_3}} = \frac{Z_3 - \sum_{i=1}^{N_{sp}} \beta_i A_{3i} Y_i^{\text{con}}}{A_{32}} = -0.00033.$$

TABLE XIII. Initial and final compositions after using Algorithms 1–4.

Species	$Y_i(t)$	$Y_i^{\text{con}}(t + \Delta t)$
CH_4	0.011	0.0080
O_2	0.031	0.0000
CO	0.045	0.0256
CO_2	0.141	0.1797
H_2	0.007	0.0060
H_2O	0.147	0.1627
N_2	(0.618)	(0.618)
$\sum_{i=1}^{N_{sp}} Y_i$	1.0000	1.0000
Y_C^E	0.0660	0.0660
Y_H^E	0.0262	0.0262
Y_O^E	0.2898	0.2898
Y_N^E	(0.6180)	(0.6180)

Now all of the new residual species mass fractions have been determined, and the composition satisfies the conservation laws. However, the mass fraction of O_2 has been predicted to be negative. This needs to be rectified.

4. Rectify final residual species if needed

The pair of species used to rectify this final residual are CO_2 and CO , i.e., $R_1 = 4$ and $R_2 = 3$, while the other element contained in these species is C , i.e., $E^R = 1$. Following Algorithm 4,

$$\begin{aligned} a &= -A_{E_{N_c} S_{N_c}} Y_{S_{N_c}}^{\text{con}} = -A_{32} Y_2^{\text{con}} = 0.00033, \\ b &= A_{O \text{CO}_2} = 0.7271, \\ c &= A_{O \text{CO}} = 0.5712, \\ d &= \frac{A_{C \text{CO}_2}}{A_{C \text{CO}}} = 0.6365, \\ \Delta Y_{R_1}^{\text{con}} &= \frac{-a}{b - cd} = -0.00091, \\ \Delta Y_{R_2}^{\text{con}} &= -d \Delta Y_{R_1}^{\text{con}} = 0.00058, \\ Y_{R_1}^{\text{con}} &= Y_{R_1}^{\text{con}} + \Delta Y_{R_1}^{\text{con}} = 0.1797, \\ Y_{R_2}^{\text{con}} &= Y_{R_2}^{\text{con}} + \Delta Y_{R_2}^{\text{con}} = 0.0256, \\ Y_{S_{N_c}}^{\text{con}} &= 0. \end{aligned}$$

The final calculated composition Y_i^{con} now satisfies all of the conservation laws with no negative predictions. The composition is summarized in Table XIII, along with the initial composition.

REFERENCES

¹T. Readshaw, T. Ding, S. Rigopoulos, and W. P. Jones, “Modeling of turbulent flames with the large eddy simulation-probability density function (LES-PDF) approach, stochastic fields, and artificial neural networks,” *Phys. Fluids* **33**, 035154 (2021).
²D. Fredrich, W. P. Jones, and A. J. Marquis, “A combined oscillation cycle involving self-excited thermo-acoustic and hydrodynamic instability mechanisms,” *Phys. Fluids* **33**, 085122 (2021).

- ³S. Ren, W. P. Jones, and X. Wang, "Stabilization mechanism revelation of a novel vortex-tube combustion technique: LES with *sgs-pdf* approach," *Phys. Fluids* **34**, 055119 (2022).
- ⁴Z. Wang, H. Wang, K. Luo, and J. Fan, "Direct numerical simulation of particle-laden turbulent boundary layers without and with combustion," *Phys. Fluids* **32**, 105108 (2020).
- ⁵H. Xiao, K. Luo, T. Jin, H. Wang, J. Xing, and J. Fan, "Direct numerical simulations of turbulent non-premixed flames: Assessment of turbulence within swirling flows," *Phys. Fluids* **33**, 015112 (2021).
- ⁶H. S. Awad, K. Abo-Amsha, U. Ahmed, M. Klein, and N. Chakraborty, "Assessment of Damköhler's hypotheses in the thin reaction zone regime using multi-step chemistry direct numerical simulations of statistically planar turbulent premixed flames," *Phys. Fluids* **34**, 055120 (2022).
- ⁷P.-D. Nguyen, H.-T. Nguyen, P. Domingo, L. Vervisch, G. Mosca, M. Gazzdallah, P. Lybaert, and V. Feldheim, "Flameless combustion of low calorific value gases, experiments, and simulations with advanced radiative heat transfer modeling," *Phys. Fluids* **34**, 045123 (2022).
- ⁸A. Mardani, B. Asadi, and A. A. Beige, "Investigation of flame structure and precessing vortex core instability of a gas turbine model combustor with different swirler configurations," *Phys. Fluids* **34**, 085129 (2022).
- ⁹P. Agostinelli, B. Rochette, D. Laera, J. Dombard, B. Cuenot, and L. Gicquel, "Static mesh adaptation for reliable large eddy simulation of turbulent reacting flows," *Phys. Fluids* **33**, 035141 (2021).
- ¹⁰A. M. Garcia, S. L. Bras, J. Prager, M. Häringer, and W. Polifke, "Large eddy simulation of the dynamics of lean premixed flames using global reaction mechanisms calibrated for CH₄-H₂ fuel blends," *Phys. Fluids* **34**, 095105 (2022).
- ¹¹Y. Sun, D. Zhao, C. Ji, T. Zhu, Z. Rao, and B. Wang, "Large-eddy simulations of self-excited thermoacoustic instability in a premixed swirling combustor with an outlet nozzle," *Phys. Fluids* **34**, 044112 (2022).
- ¹²A. Péquin, S. Iavarone, R. M. Galassi, and A. Parente, "The partially stirred reactor model for combustion closure in large eddy simulations: Physical principles, sub-models for the cell reacting fraction, and open challenges," *Phys. Fluids* **34**, 055122 (2022).
- ¹³J.-Y. Chen, W. Kollmann, and R. Dibble, "Pdf modeling of turbulent nonpremixed methane jet flames," *Combust. Sci. Technol.* **64**, 315–346 (1989).
- ¹⁴S. Pope, "Computationally efficient implementation of combustion chemistry using in situ adaptive tabulation," *Combust. Theory Modell.* **1**, 41–63 (1997).
- ¹⁵N. Peters, *Turbulent Combustion* (Cambridge University Press, 2000).
- ¹⁶M. Ihme, W. T. Chung, and A. A. Mishra, "Combustion machine learning: Principles, progress and prospects," *Prog. Energy Combust. Sci.* **91**, 101010 (2022).
- ¹⁷A. Kempf, F. Flemming, and J. Janicka, "Investigation of lengthscales, scalar dissipation, and flame orientation in a piloted diffusion flame by LES," *Proc. Combust. Inst.* **30**, 557–565 (2005).
- ¹⁸M. Ihme and H. Pitsch, "Modeling of radiation and nitric oxide formation in turbulent nonpremixed flames using a flamelet/progress variable formulation," *Phys. Fluids* **20**, 055110 (2008).
- ¹⁹M. Ihme, C. Schmitt, and H. Pitsch, "Optimal artificial neural networks and tabulation methods for chemistry representation in LES of a bluff-body swirl-stabilized flame," *Proc. Combust. Inst.* **32**, 1527–1535 (2009).
- ²⁰M. Hansinger, Y. Ge, and M. Pfitzner, "Deep residual networks for flamelet/progress variable tabulation with application to a piloted flame with inhomogeneous inlet," *Combust. Sci. Technol.* **194**, 1587–1613 (2020).
- ²¹F. Christo, A. Masri, E. Nebot, and S. Pope, "An integrated PDF/neural network approach for simulating turbulent reacting systems," *Symp. (Int.) Combust.* **26**, 43–48 (1996).
- ²²F. Christo, A. Masri, E. Nebot, and T. Turanyi, "Utilizing artificial neural network and repro-modelling in turbulent combustion," in IEEE International Conference on Neural Networks - Conference Proceedings (1995).
- ²³F. Christo, A. Masri, and E. Nebot, "Artificial neural network implementation of chemistry with PDF simulation of H₂/CO₂ flames," *Combust. Flame* **106**, 406–427 (1996).
- ²⁴J. Blasco, N. Fueyo, C. Dopazo, and J. Ballester, "Modelling the temporal evolution of a reduced combustion chemical system with an artificial neural network," *Combust. Flame* **113**, 38–52 (1998).
- ²⁵J. Blasco, N. Fueyo, J. Larroya, C. Dopazo, and J.-Y. Chen, "A single-step time-integrator of a methane-air chemical system using artificial neural networks," *Comput. Chem. Eng.* **23**, 1127–1133 (1999).
- ²⁶N. Mehdizadeh, P. Sinaei, and A. Nichkoobi, "Modeling Jones' reduced chemical mechanism of methane combustion with artificial neural network," in ASME 3rd Joint US-European Fluids Engineering Summer Meeting (2010).
- ²⁷B. Sen and S. Menon, "Linear eddy mixing based tabulation and artificial neural networks for large eddy simulations of turbulent flames," *Combust. Flame* **157**, 62–74 (2010).
- ²⁸B. Sen, E. Hawkes, and S. Menon, "Large eddy simulation of extinction and reignition with artificial neural networks based chemical kinetics," *Combust. Flame* **157**, 566–578 (2010).
- ²⁹A. Chatzopoulos and S. Rigopoulos, "A chemistry tabulation approach via rate-controlled constrained equilibrium (RCCE) and artificial neural networks (ANNs), with application to turbulent non-premixed CH₄/H₂/N₂ flames," *Proc. Combust. Inst.* **34**, 1465–1473 (2013).
- ³⁰L. Franke, A. Chatzopoulos, and S. Rigopoulos, "Tabulation of combustion chemistry via artificial neural networks (ANNs): Methodology and application to LES-PDF simulation of Sydney flame L," *Combust. Flame* **185**, 245–261 (2017).
- ³¹T. Ding, T. Readshaw, S. Rigopoulos, and W. P. Jones, "Machine learning tabulation of thermochemistry in turbulent combustion: An approach based on hybrid flamelet/random data and multiple multilayer perceptrons," *Combust. Flame* **231**, 111493 (2021).
- ³²T. Ding, S. Rigopoulos, and W. P. Jones, "Machine learning tabulation of thermochemistry of fuel blends," *Appl. Energy Combust. Sci.* **12**, 100086 (2022).
- ³³K. Wan, C. Barnaud, L. Vervisch, and P. Domingo, "Chemistry reduction using machine learning trained from non-premixed micro-mixing modeling: Application to DNS of a syngas turbulent oxy-flame with side-wall effects," *Combust. Flame* **220**, 119–129 (2020).
- ³⁴P. Nguyen, H. Domingo, L. Vervisch, and D. Nguyen, "Machine learning for integrating combustion chemistry in numerical simulations," *Energy AI* **5**, 100082 (2021).
- ³⁵M. Haghshenas, P. Mitra, N. Dal Santo, and D. P. Schmidt, "Acceleration of chemical kinetics computation with the learned intelligent tabulation (LIT) method," *Energies* **14**, 7851 (2021).
- ³⁶R. Laubscher and J. Hoffman, "Utilization of basic multi-layer perceptron artificial neural networks to resolve turbulent fine structure chemical kinetics applied to a CFD model of a methane/air piloted jet flame," *J. Therm. Eng.* **4**, 1828–1846 (2018).
- ³⁷C. Cheng, G. Janiga, and D. Thévenin, "On-the-fly artificial neural network for chemical kinetics in direct numerical simulations of premixed combustion," *Combust. Flame* **226**, 467–477 (2021).
- ³⁸O. Owoyele, P. Kundu, M. Ameen, T. Echehki, and S. Som, "Application of deep artificial neural networks to multi-dimensional flamelet libraries and spray flames," *Int. J. Engine Res.* **21**, 151–168 (2020).
- ³⁹T. Beucler, M. Pritchard, S. Rasp, J. Ott, P. Baldi, and P. Gentine, "Enforcing analytic constraints in neural networks emulating physical systems," *Phys. Rev. Lett.* **126**, 098302 (2021).
- ⁴⁰T. Bolton and L. Zanna, "Applications of deep learning to ocean data inference and subgrid parameterization," *J. Adv. Model. Earth Syst.* **11**, 376–399 (2019).
- ⁴¹K. Wan, C. Barnaud, L. Vervisch, and P. Domingo, "Machine learning for detailed chemistry reduction in DNS of a syngas turbulent oxy-flame with side-wall effects," *Proc. Combust. Inst.* **38**, 2825–2833 (2021).
- ⁴²M. Frenklach, H. Wang, M. Goldenberg, G. Smith, D. Golden, C. Bowman, R. Hanson, W. Gardiner, and V. Lissianski, "GRI-Mech—An optimized detailed chemical reaction mechanism for methane combustion," Report No. PB-96-137054/XAB (Gas Research Institute, 1995).
- ⁴³H. Wang, X. You, A. V. Joshi, S. G. Davis, A. Laskin, F. Egoopoulos, and C. K. Law, see http://ignis.usc.edu/USC_Mech_II.htm for "USC Mech Version II. High-temperature combustion reaction model of H₂/CO/C1-C4 compounds" (2007) (accessed September 27, 2022).
- ⁴⁴M. Hagan, H. Demuth, M. Beale, and O. D. Jess, *Neural Network Design* (Martin Hagan, 2014).

- ⁴⁵M. Bode, M. Guading, Z. Lian, D. Denker, M. Davidovic, K. Kleinheinz, J. Jitsev, and H. Pitsch, "Using physics-informed enhanced super-resolution generative adversarial networks for subfilter modeling in turbulent reactive flows," *Proc. Combust. Inst.* **38**, 2617–2625 (2021).
- ⁴⁶P. Brown, G. Byrne, and A. Hindmarsh, "VODE: A variable-coefficient ODE solver," *SIAM J. Sci. Stat. Comput.* **10**, 1038–1051 (1989).
- ⁴⁷W. P. Jones and S. Rigopoulos, "Reduced chemistry for hydrogen and methanol premixed flames via RCCE," *Combust. Theory Modell.* **11**, 755–780 (2007).
- ⁴⁸D. Marquardt, "An algorithm for least squares estimation of nonlinear parameters," *SIAM J. Appl. Math.* **11**, 431–441 (1963).
- ⁴⁹W. Jones and R. Lindstedt, "Global reaction schemes for hydrocarbon combustion," *Combust. Flame* **73**, 233–249 (1988).